Journal of Alloys and Compounds 597 (2014) 230–235

Contents lists available at ScienceDirect

Journal of Alloys and Compounds

journal homepage: www.elsevier.com/locate/jalcom

Modelling high-power spin-torque oscillator with perpendicular magnetization in half-metallic Heusler alloy spin valve nanopillar

H.B. Huang [a,b,*], X.Q. Ma [a], Z.H. Liu [a], L.Q. Chen [b]

[a] Department of Physics, University of Science and Technology Beijing, Beijing 100083, China
[b] Department of Materials Science and Engineering, The Pennsylvania State University, University Park, PA 16802, USA

ARTICLE INFO

Article history:
Received 27 November 2013
Received in revised form 30 January 2014
Accepted 31 January 2014
Available online 8 February 2014

Keywords:
Micromagnetic simulation
Spin torque oscillator
Heusler alloy
Spin-valve nanopillar
Magnetization precession

ABSTRACT

We investigated the high-power spin-torque oscillator in a half-metallic Heusler alloy Co_2MnSi spin-valve nanopillars with perpendicular magnetization using micromagnetic simulations. A stable high output power spin transfer precession was obtained in the condition of zero external magnetic field, and the narrow current of oscillation due to the high spin polarization of Heusler alloy is significantly widened by introducing the surface anisotropy. Furthermore, we discussed the current dependence of oscillation frequency and explained the blue frequency shift using the trajectories and spatial magnetic domains.

1. Introduction

Spin transfer torque (STT) [1,2] resulted from the transfer of angular momentums from the spin-polarized electrons to the ferromagnetic magnetization, and it could be applied to exploit the possible applications in future spintronics. The magnetization precession could be produced when STT input equals to the magnetic damping torque. The high frequency precession has been investigated in the multilayers in both spin valve nanopillar [3] and point contact geometries [4]. Coupled with the giant magnetoresistance effect (GMR), this stable precession produces a voltage response that makes these devices high-frequency oscillators, called spin torque oscillators (STO). STO has various attractive advantages, e.g., high frequency microwave (2–100 GHz), narrow output band with high Q values (>10,000), tunable over a wide range of frequencies via applied field or current, and voltage outputs in the mV regime. However, it is difficult to increase the output power and maintain narrow oscillation linewidth for any useful applications. There were many attempts to increase the output power, e.g., a magnetic tunnel junction (MTJ) STO [5,6]. It is demonstrated that MTJ–STO increases the output power but widens the linewidth. Compared with MTJ–STO, the advantages of using a full metal STO are their narrow linewidth and low resistance enabling good impedance matching. However, the lower output power of metal STO is the biggest problem for designing applicable devices. Recently, the high polarization materials like Heusler alloys are used, it could increase GMR signal [7,8] and hence the power output from the oscillator.

Heusler alloys have lower saturation magnetization M_s [9], smaller Gilbert damping constant α [10], higher spin polarization factor η [11] and higher GMR ratio [12]. In the experiments, a large MR ratio of 12.5% can be obtained in Co_2MnSi (CMS) alloy arising from its large spin polarization, and a high rf output power of 1.1 nW was achieved in spite of a small precession angle of 8.6° of in-plane precession mode [13]. A large emission amplitudes exceeding 150 nV/Hz and narrow linewidth below 10 MHz was obtained by setting the external magnetic field magnitude or angle and current to an optimum value [14]. We have already demonstrated that the output power could be improved significantly due to the out-of-plane precession (OPP) by using micromagnetic simulation [15]. However, the realization of the high power STO depends on the specific conditions, such as, external magnetic field and optimum current. Using an out-of-plane magnetized polarizer of the fixed layer has been demonstrated to get stable OPP mode at the critical current without external magnetic field. Therefore, the same magnetization structure with the perpendicular magnetization is adopted in the half-Heusler alloy spin valve nanopillars to get the high output power. Furthermore, the narrowing optimum current region for the rf oscillation due to the high spin

* Corresponding author at: Department of Materials Science and Engineering, The Pennsylvania State University, University Park, PA 16802, USA. Tel.: +1 8143084681.
E-mail address: houbinghuang@gmail.com (H.B. Huang).

http://dx.doi.org/10.1016/j.jallcom.2014.01.235
0925-8388/

polarization constant of Heusler alloy is the barrier to get the stable OPP oscillation which is demonstrated by Seki et al. using macrospin model [16]. Since the balance between STT and the damping torque is the key to stabilize the precessional oscillation, the magnitude of the effective field is not sufficiently large to compete with the large STT originating from the high spin polarization constant in Heusler-based spin valve nanopillars. In addition, the surface and interfacial anisotropies are non-negligible and often dominate the bulk contributions in the ultrathin films. It was demonstrated that the interfacial perpendicular anisotropy decreases the critical current of spin transfer magnetization switching in MgO-based magnetic tunnel junction nanopillars with perpendicular full-Heusler alloy electrodes [17]. Thus the surface anisotropy which is characterized by the thin film roughness also plays a vital role in STT induced magnetization dynamics [18,19]. In this paper, we investigated the high power STO of CMS Heusler alloy with the perpendicular polarization by introducing a surface anisotropy. We argue that one can utilize the surface anisotropy to increase the magnitude of effective field and thus broaden the current region for the high output power oscillation.

2. Theoretical model

As showed in Fig. 1 (left), a Cartesian coordinate system is employed where the x-axis and y-axis are the long-axis and short-axis of the ellipse. A CMS-based spin valve device with the structure of CMS (16 nm)/Ag (4 nm)/CMS (2 nm) and the elliptical cross section area of $100 \times 76\ \mathrm{nm}^2$ is studied by using micromagnetic simulations. The two CMS layers are separated by a thin Ag layer, and the top CMS layer is the free layer whose magnetization dynamics is triggered by a spin-polarized current. The bottom CMS layer is the reference layer with the magnetization **P** along the positive z axis. In our simulation, the current will be polarized perpendicularly to the plane of the pillar by the perpendicular magnetization of the reference layer. A positive current is defined as a current flowing from the free layer to the reference layer. The initial magnetization vector **M** of the free layer is along the negative z axis. After the electrons go through the reference layer, the spin transfer torque will act on the free layer magnetization. At a small current density, the damping torque will push **M** back toward the low energy configuration along the negative z axis. With the increase current density, a stable magnetization precession will be produced as STT input equals to the magnetic damping torque. (Right) At the end, the magnetization will switch to another stable configuration along the positive z axis if the current is large enough to overcome the energy barrier.

We describe the dynamics of **M** using a generalized Landau–Lifshitz–Gilbert–Slonczewski (LLGS) equation [1],

$$\frac{d\mathbf{M}}{dt} = -\gamma'\mathbf{M}\times\mathbf{H}_{\mathrm{eff}} - \frac{\alpha\gamma'}{M_s}\mathbf{M}\times(\mathbf{M}\times\mathbf{H}_{\mathrm{eff}}) - \frac{2\mu_B J}{(1+\alpha^2)edM_s^3}g(\mathbf{M},\mathbf{P})\mathbf{M}\times(\mathbf{M}\times\mathbf{P}) + \frac{2\mu_B\alpha J}{(1+\alpha^2)edM_s^2}g(\mathbf{M},\mathbf{P})(\mathbf{M}\times\mathbf{P}) \quad (1)$$

where the effective field $\mathbf{H}_{\mathrm{eff}}$ could be expressed by $\mathbf{H}_{\mathrm{eff}} = -\frac{1}{\mu_0}\frac{\delta E}{\delta \mathbf{M}}$, $\gamma' = \gamma/(1+\alpha^2)$, γ is the electron gyromagnetic ratio, and α is the dimensionless damping parameter. The last two terms on the right side of Eq. (1) describe STT which tends to drag the magnetization away from its initial state and drives the magnetization precession. μ_B, J, d, e, M_s, are the Bohr magnetron, the current density, the thickness of the free layer, the electron charge and the saturation magnetization, respectively. Here, we only consider the first term of transverse torque and ignore the second term of smaller field-like torque since the field-like torque is very small in metallic alloys [17,18].

The scalar function $g(\mathbf{M}, \mathbf{P})$ is given by [1]

$$g(\mathbf{M},\mathbf{P}) = \left[-4 + (1+\eta)^3(3+\mathbf{M}\cdot\mathbf{P}/M_s^2)/4\eta^{3/2}\right]^{-1} \quad (2)$$

where η is the spin polarization factor, the angle between **M** and **P** is θ. $\mathbf{M}\cdot\mathbf{P}/M_s^2 = \cos\theta$. The total effective fields include magnetocrystalline anisotropy, surface anisotropy, demagnetization, external magnetic, and exchange fields, namely,

$$\mathbf{H}_{\mathrm{eff}} = \mathbf{H}_{\mathrm{anis}} + \mathbf{H}_{\mathrm{surf}} + \mathbf{H}_{\mathrm{d}} + \mathbf{H}_{\mathrm{ext}} + \mathbf{H}_{\mathrm{ex}} \quad (3)$$

Different with the previous model, we introduce the shape anisotropy energy [19,20], $\mathbf{H}_{\mathrm{surf}} = K_s m_z^2/d$, where K_s is surface anisotropy constant. The expressions of other energies could be found in our previous paper [21–24]. The effective field should significantly increase by adding the term of $\mathbf{H}_{\mathrm{surf}}$, and it will overcome the large STT input and produce the high power oscillation.

The dynamics of magnetization is investigated by numerically solving the time-dependent LLGS equation using the Gauss–Seidel projection method [25] with a constant time step $\Delta t = 0.0268858$ ps [26]. We adopted the following magnetic parameters, saturation magnetization $M_s = 8.0 \times 10^5$ A/m [27] smaller than the experimental value for thinner thickness, exchange constant $A = 2.0 \times 10^{-11}$ J/m [28], magnetocrystalline anisotropy constant $K_1 = 3.0 \times 10^3$ J/m^3 [29], and surface anisotropy constant $K_s = -1.3 \times 10^6$ J/m^3 [19,20]. Other parameters are

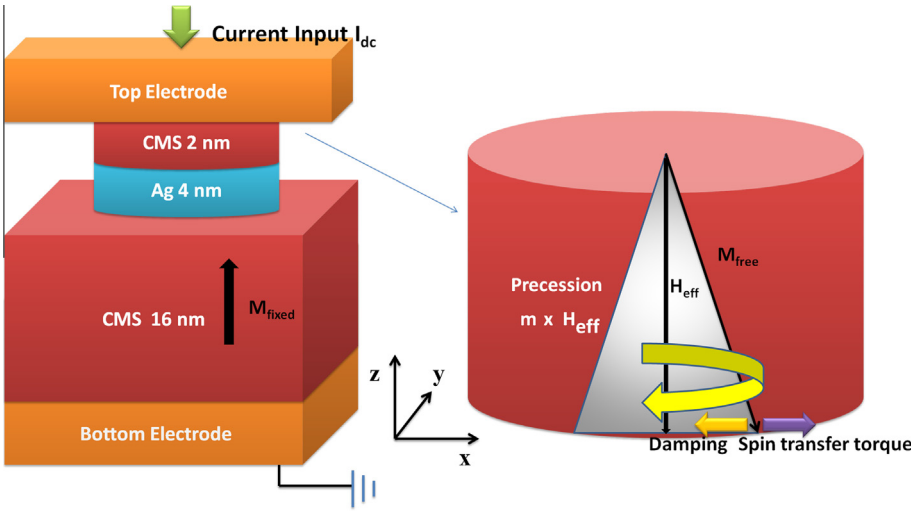

Fig. 1. Schematic illustration of Co_2MnSi (CMS)/Ag/CMS spin valve nanopillar (left). Directions of damping and spin transfer torque vectors in the free layer (right).

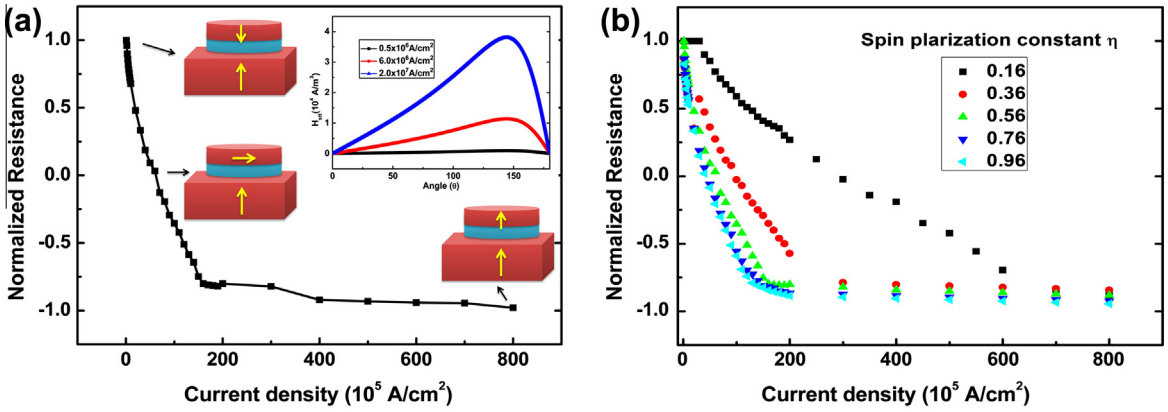

Fig. 2. (a) Normalized resistances as a function of current density (*R–J*) of CMS/Ag/CMS spin valve nanopillar. Inset shows the relationships of STT vs θ in Slonczewski's model at different current densities. (b) Normalized resistances as a function of current density (*R–J*) of CMS/Ag/CMS spin valve nanopillar at different spin polarization constants.

Gilbert damping parameter $\alpha = 0.008$, [10] spin polarization factor $\eta = 0.56$, [30] and electron gyromagnetic ratio $\gamma = 2.3245 \times 10^5$ m/(A s). Additionally, the easy axis was along [100], [010] and [001], however the easy axis is along [001] after introducing the surface anisotropy. Furthermore, the output power is obtained from the Fourier transformation of magnetization components oscillation $M_z(t)$ expressed by,

$$F(w) = F(M_z(t)) = \int_{-\infty}^{\infty} M_z(t) e^{-iwt}\, dt \tag{4}$$

where ω is the angular frequency and expressed by $\omega = 2\pi f$ with f the frequency.

3. Results and discussion

We investigated the high power STO with perpendicular magnetization reference layer by introducing the surface anisotropy in the free layer of a half-Heusler CMS alloy spin-valve nanopillar by using micromagnetic simulations. Fig. 2(a) shows normalized resistances as a function of current density (*R–J*) of CMS/Ag/CMS spin valve nanopillar. The definition of normalized resistance could be expressed by $R = 2r/(R_{AP} - R_P) - (R_{AP} + R_P)/(R_{AP} - R_P)$, where r is the real resistance. With the increase of current density, the resistance is decreasing from the high resistance state of anti-parallel configuration to the low resistance state of parallel configuration. For example, the normalized resistances are 0.815 and 0.032 at the current densities of 0.5×10^6 A/cm^2 and 6.0×10^6 A/cm^2, respectively. The normalized resistance equals to -0.801 at the current density of 20.0×10^6 A/cm^2. Based on the slope of the reduced resistance curve, we separate the dynamics of magnetization into two stages: stable precessional stage and pre-switching stage. In the stable precessional stage, the normalized resistance reduces rapidly before the critical current density of 16.0×10^6 A/cm^2. In the pre-switching stage, the magnitude of the reduced resistance is smaller than the stable precessional stage. These characteristics can be elucidated by Slonczewski's model[1], which takes into account the interface spin-flip scattering between the layers. In this model, STT could be described by $\mathbf{H}_{stt} = 2\mu_B J_g(\mathbf{M}, \mathbf{P})(\mathbf{M} \times \mathbf{P})/(\gamma e d M_s^3)$. As shown in the inset of Fig. 2(a), $\mathbf{H}_{stt}$ is proportional to J and $g(\theta)$. If the angle is larger than the threshold angle of 37°, $\mathbf{H}_{stt}$ depends primarily on the current density. If the angle is smaller than 37°, $\mathbf{H}_{stt}$ depends on $g(\theta)$. Therefore, the resistance reduces rapidly because of the increase of the current density in the stable precessional stage. In the pre-switching stage, the fact that the resistance almost does not change with the increase of the current density is resulted from the small $g(\theta)$ when the angle is smaller than the critical angle of 37°. The normalized resistance at the negative current density is not shown, because we focus on the stable magnetization precession which was only found in the positive current density under zero magnetic field [3,31,32]. As shown in Fig. 2(b), *R–J* curves at different spin polarization constants indicate that the range of oscillation is decreasing with the increase of spin polarization constants. However the oscillation could be obtained at a wide range of current from 0.1×10^6 A/cm^2 to 10.0×10^6 A/cm^2, even though the spin polarization constant increases to 0.96. Therefore, the stable precessional stage could be obtained in a wide range of current density in the CMS-based STO with perpendicular polarized magnetization reference layer by introducing the surface anisotropy without the external magnetic field, which provide an effective way to broaden the current range of oscillation in Heusler-based spin valve with a larger spin polarization constant [16].

Fig. 3(a)–(c) shows the evolutions of magnetization components $\langle m_z \rangle$, $\langle m_x \rangle$ and $\langle m_y \rangle$ under different current densities, respectively. The magnetizations have precession about the axis of the effective field when the system reaches to the balance between STT and the magnetic damping torque after several nanoseconds. The time of reaching to the balance reduces with the increase of the current density. In those cases after reaching to the balance, STT which always equals to the magnetic damping torque excites coherent precession. For example, the $\langle m_z \rangle$ of blue[1] curve is -0.355 at the current density of 10.0×10^6 A/cm^2 when the dynamics reach to the balance after 5.0 ns. Although $\langle m_z \rangle$ does not change after reaching to the balance, $\langle m_x \rangle$ and $\langle m_y \rangle$ are oscillating after reaching to the balance state. We could observe this effect from the blue curves of Fig. 3(b) and (c), the sine curves of $\langle m_x \rangle$ and $\langle m_y \rangle$ oscillations reach to the minimum and maximum at the time of 5.004 ns. Furthermore, the period is decreasing with the increase of the current density. The periods are 0.084 ns and 0.032 ns at the current densities of 1.0×10^6 A/cm^2 and 6.0×10^6 A/cm^2, respectively. The frequencies are 11.9 GHz and 31.2 GHz. As the current increases to 20.0×10^6 A/cm^2, the magnetization configuration is close to parallel structure and $\mathbf{H}_{stt}$ is small. We observed that the magnetization is oscillating rapidly and the frequency is high significantly, however we could not obtain the single frequency oscillation due to the excitation of non-uniform magnetization precession.

Fig. 4(a) shows the power spectral density (PSD) with the increase of current densities. For clarity, all the spectra are shifted

[1] For interpretation of color in Figs. 3 and 4, the reader is referred to the web version of this article.

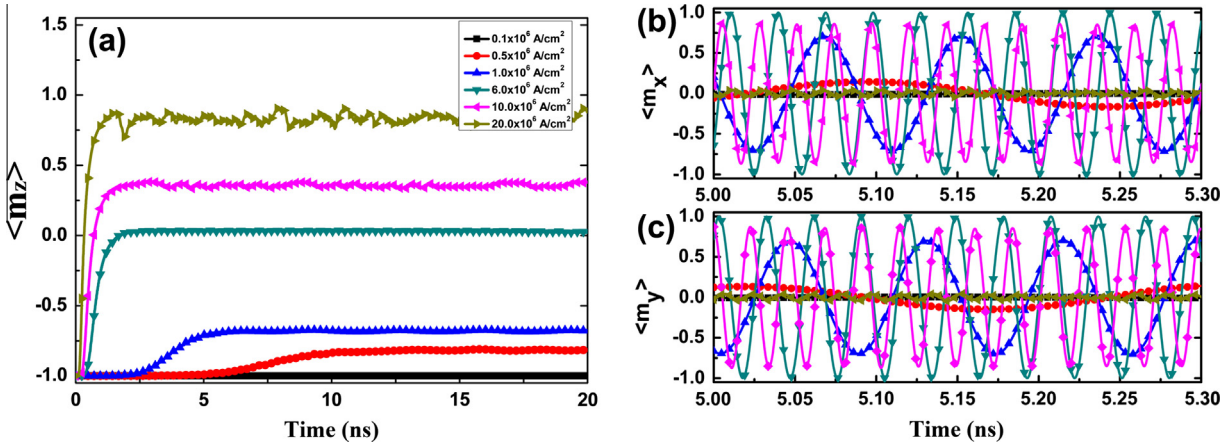

Fig. 3. (a–c) Evolutions of magnetization component $\langle m_z \rangle$, $\langle m_x \rangle$ and $\langle m_y \rangle$ under different current densities, respectively.

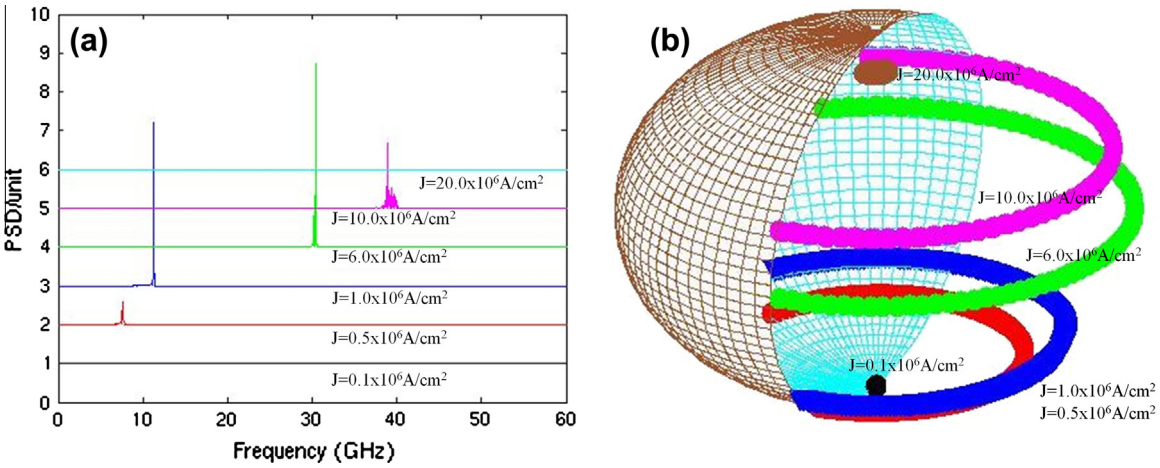

Fig. 4. (a) PSD as the increase of current densities. For clarity, spectra are shifted vertically with different constants. (b) Trajectories of spin-transfer torque driven dynamics for the magnetization vector under different current densities.

vertically by different constants. As the current density increases from 0.5×10^6 A/cm^2 to 10.0×10^6 A/cm^2, the frequencies are increasing (blue shift) from 8.1 GHz to 39.5 GHz except no stable precession at the lowest and highest current densities of 0.1×10^6 A/cm^2 and 20.0×10^6 A/cm^2. In fact, the frequency for the out-of-plane precession can be estimated by [1,33,34],

$$f \approx \frac{\gamma}{2\pi}\left[\frac{\hbar}{2e}\frac{g(\eta)}{M_s d}\right]\frac{J}{\alpha} \tag{5}$$

From the approximate Eq. (5), the increase of the frequency with the current density becomes evident. Different with our previous results of in-plane free layer magnetization under the external magnetic field, the second harmonic signal is not observed since the output voltage is predominantly proportional to $\langle m_z \rangle$ [15]. Additionally, the linewidth of oscillation at the current density of 10.0×10^6 A/cm^2 is wider than the linewidth at the small current densities. The amplitudes of oscillations at the current densities of 1.0×10^6 A/cm^2 and 6.0×10^6 A/cm^2 are higher than the others. The high output power of oscillation with the narrow linewidth could be fulfilled by the appropriate current range from 1.0×10^6 A/cm^2 to 6.0×10^6 A/cm^2. Fig. 4(b) shows the trajectories under the different current densities from 0.5×10^6 A/cm^2 to 10.0×10^6 A/cm^2.

Fig. 5(a) shows phase diagram of power spectral density indicating the frequency as a function of applied current. The colors represent the magnitude of output power. The frequency is increasing with the current, which could be explained by Eq. (5). However, our previous results showed that the frequency of IPP was decreasing with the current. The difference of frequency dependences between IPP and OPP indicate that the current have different attributions for magnetization precession. The maximum of output power could be obtained at the current density of 7.5×10^6 A/cm^2. Fig. 5(b) shows the magnetic domains at different current densities of 0.1×10^6 A/cm^2, 6.0×10^6 A/cm^2, and 15.0×10^6 A/cm^2. The colors represent the magnitude of the magnetization components $\langle m_z \rangle$(−1.0 to 1.0) while the arrows indicate the in-plane magnetization. Domains are characterized as a precession of the arrows. The magnetization at each point of the free layer experiences a torque exerted by the STT, with its magnitude being decided by the angle θ between **M** and **P**. At a small current of 0.1×10^6 A/cm^2, the magnetization is along the negative z axis. As the current increases to 6.0×10^6 A/cm^2, the magnetizations precess along the effective field and the maximum power could be obtained. Then the magnetization is along the positive z axis as the current increases to 15.0×10^6 A/cm^2.

Fig. 6(a)–(f) shows the magnetization trajectories and oscillation evolutions with different surface anisotropy constants of $K_s = 0$, $K_s = -1.3 \times 10^3$ J/m^3 and $K_s = -1.3 \times 10^6$ J/m^3, respectively. For the case of $K_s = 0$, unstable trajectories are obtained due to the high spin polarization constant of Heusler alloys, and no stable oscillation of magnetization evolutions was observed (Fig. 6(a) and

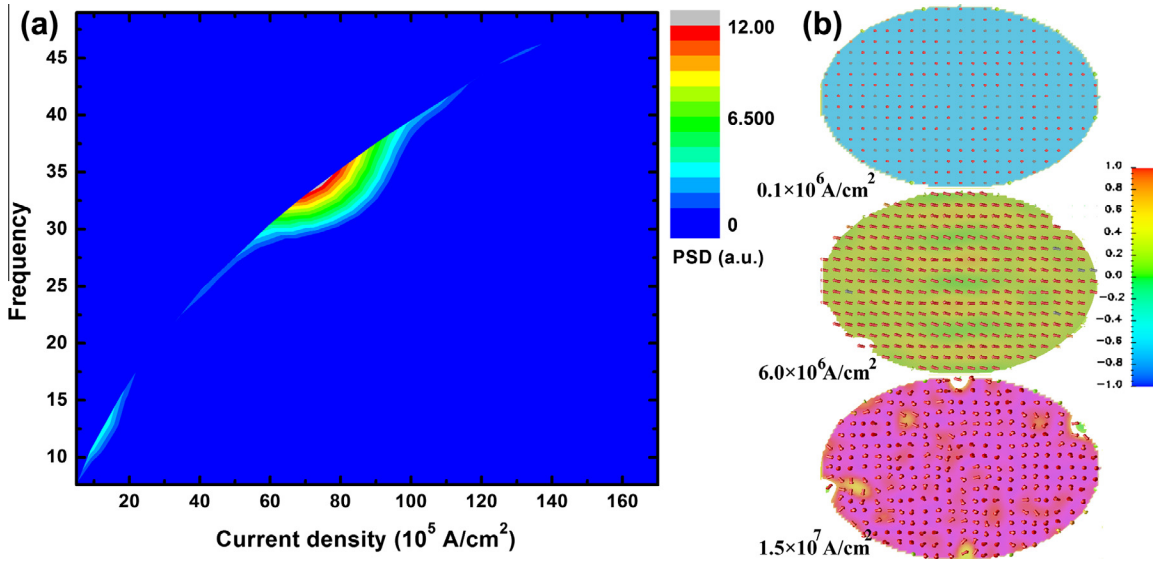

Fig. 5. (a) Phase diagram of power spectral density showing the frequency as a function of applied current. The colors represent the magnitude of output power. (b) Oscillation domains at different current densities. (For interpretation of the references to colour in this figure legend, the reader is referred to the web version of this article.)

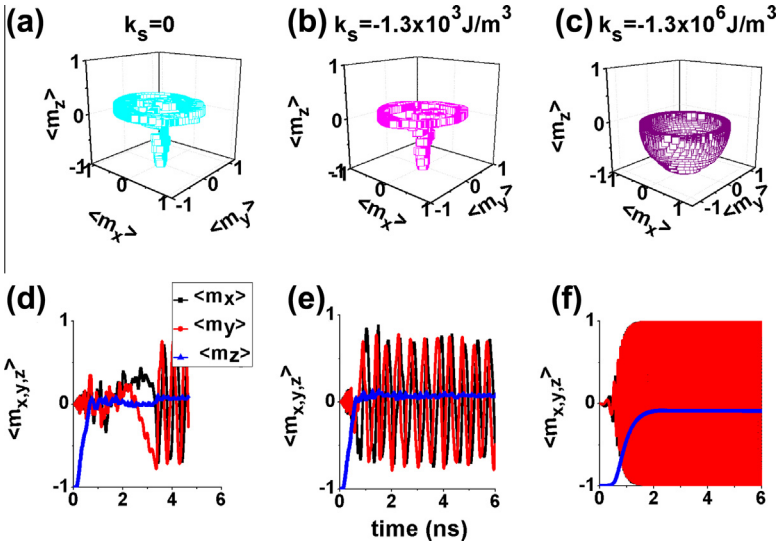

Fig. 6. (a)–(c) The magnetization trajectories and (d)–(f) oscillation evolutions with different surface anisotropy constants of $K_s = 0$, $K_s = -1.3 \times 10^3$ J/m^3 and $K_s = -1.3 \times 10^6$ J/m^3, respectively.

(d)). Since the magnitude of the effective field is not sufficiently large to compete with the large STT originating from the high spin polarization constant in Heusler-based spin valve nanopillars, larger STT input destroys the balance between STT and Gilbert damping and leads to the unstable magnetization precession. However, after introducing the surface anisotropy in the effective field with $K_s = -1.3 \times 10^3$ J/m^3 and $K_s = -1.3 \times 10^6$ J/m^3, STT input induces the stable magnetization precession around the effective field. In addition, the current range of oscillation increases with the surface anisotropy. Those results provide an effective way to solve the narrow current range for spin torque oscillation in Heusler-based spin valve nanopillars.

4. Conclusions

In summary, we investigated the high-power STT with perpendicular polarization in a half-metallic Heusler alloy Co_2MnSi (CMS) spin-valve nanopillars using micromagnetic simulations. We obtained the high output power spin transfer precession at a wide range of current density by introducing the surface anisotropy in the condition of zero external magnetic field even though with the high spin polarization constant. We divided the magnetization dynamics into two stages: stable precessional stage and pre-switching stage, and both of them were explained by Slonczewski's model. The current dependence of the out-of-plane precession oscillation frequency is quite different from that of the in-plane precession. We demonstrated that the frequency increases linearly with the current, which could be explained by using the trajectories and spatial magnetic domains.

Acknowledgements

This work was sponsored by the National Science Foundation of China (11174030), by the US National Science Foundation under the Grant Number DMR-1006541 (Chen and Huang). The computer simulations were carried out on the LION and Cyberstar clusters at the Pennsylvania State University.

References

[1] J.C. Slonczewski, J. Magn. Magn. Mater. 159 (1996) L1.
[2] L. Berger, Phys. Rev. B 54 (1996) 9359.
[3] S.I. Kiselev, J.C. Sankey, I.N. Krivorotov, N.C. Emley, R.J. Schoelkopf, R.A. Buhrman, D.C. Ralph, Nature 425 (2003) 380.
[4] W.H. Rippard, M.R. Pufall, S. Kaka, S.E. Russek, T.J. Silva, Phys. Rev. Lett. 92 (2004) 027201.
[5] A.M. Deac, A. Fukushima, H. Kubota, H. Maehara, Y. Suzuki, S. Yuasa, Y. Nagamine, K. Tsunekawa, D.D. Djayaprawira, N. Watanabe, Nat. Phys. 4 (2008) 803.
[6] Z.M. Zeng, P. Upadhyaya, P.K. Amiri, K.H. Cheung, J.A. Katine, J. Langer, K.L. Wang, H.W. Jiang, Appl. Phys. Lett. 99 (2011) 032503.
[7] H. Wang, A. Sato, K. Saito, S. Mitani, K. Takanashi, K. Yakushiji, Appl. Phys. Lett. 90 (2007) 142510.
[8] N. Tezuka, N. Ikeda, S. Sugimoto, K. Inomata, Appl. Phys. Lett. 89 (2006) 252508.
[9] O. Gaier, J. Hamrle, S.J. Hermsdoerfer, H. Schultheiβ, B. Hillebrands, Y. Sakuraba, M. Oogane, Y. Ando, J. Appl. Phys. 103 (2008) 103910.
[10] R. Yilgin, M. Oogane, Y. Ando, T. Miyazaki, J. Magn. Magn. Mater. 310 (2007) 2322.
[11] R. Shan, H. Sukegawa, W. Wang, M. Kodzuka, T. Furubayashi, T. Ohkubo, S. Mitani, K. Inomata, K. Hono, Phys. Rev. Lett. 102 (2009) 246601.
[12] W. Wang, H. Sukegawa, R. Shan, S. Mitani, K. Inomata, Appl. Phys. Lett. 95 (2009) 182502.
[13] R. Okura, Y. Sakuraba, T. Seki, K. Izumi, M. Mizuguchi, K. Takanashi, Appl. Phys. Lett. 99 (2011) 052510.
[14] J. Sinha, M. Hayashi, Y.K. Takahashi, T. Taniguchi, M. Drapeko, S. Mitani, K. Hono, Appl. Phys. Lett. 99 (2011) 162508.
[15] H.B. Huang, X.Q. Ma, Z.H. Liu, C.P. Zhao, L.Q. Chen, AIP Adv. 3 (2013) 032132.
[16] T. Seki, Y. Sakuraba, R. Okura, K. Takanashi, J. Appl. Phys. 113 (2013) 033907.
[17] M.A. Zimmler, B. Özyilmaz, W. Chen, A.D. Kent, J.Z. Sun, M.J. Rooks, R.H. Koch, Phys. Rev. B 70 (2004) 184438.
[18] H. Meng, J.P. Wang, Appl. Phys. Lett. 88 (2006) 172506.
[19] N.A. Pertsev, H. Kohlstedt, Adv. Funct. Mater. 10 (2012) 1002.
[20] M. Rewienski, Acta Phys. Pol., A 88 (1995) S69.
[21] Z.H. Xiao, X.Q. Ma, P.P. Wu, J.X. Zhang, L.Q. Chen, S.Q. Shi, J. Appl. Phys. 102 (2007) 093907.
[22] H.B. Huang, X.Q. Ma, Z.H. Liu, F.Y. Meng, Z.H. Xiao, P.P. Wu, S.Q. Shi, L.Q. Chen, J. Appl. Phys. 110 (2011) 033913.
[23] H.B. Huang, X.Q. Ma, Z.H. Liu, F.Y. Meng, S.Q. Shi, L.Q. Chen, J. Magn. Magn. Mater. 330 (2013) 16.
[24] H.B. Huang, X.Q. Ma, Z.H. Liu, C.P. Zhao, S.Q. Shi, L.Q. Chen, Appl. Phys. Lett. 102 (2013) 042405.
[25] X.P. Wang, C.J. García-Cervera, E. Weinan, J. Comput. Phys. 171 (2001) 357.
[26] H.B. Huang, X.Q. Ma, T. Yue, Z.H. Xiao, S.Q. Shi, L.Q. Chen, Mech. Phys. 54 (2011) 1227.
[27] B. Balke, G.H. Fecher, H.C. Kandpal, C. Felser, K. Kobayashi, E. Ikenaga, J.J. Kim, S. Ueda, Phys. Rev. B 74 (2006) 104405.
[28] J. Hamrle, O. Gaier, S.G. Min, B. Hillebrands, Y. Sakuraba, Y. Ando, J. Appl. Phys. 42 (2009) 084005.
[29] R. Yilgin, Y. Sakuraba, M. Oogane, S. Mizumaki, Y. Ando, T. Miyazaki, Jpn. J. Appl. Phys. 46 (2007) L205.
[30] L. Ritchie, G. Xiao, Y. Ji, T.Y. Chen, C.L. Chien, M. Zhang, J.L. Chen, Z.H. Liu, G.H. Wu, X.X. Zhang, Phys. Rev. B 68 (2003) 104430.
[31] X.Q. Ma, Z.H. Xiao, P.P. Wu, J.X. Zhang, S.Q. Shi, L.Q. Chen, J. Appl. Phys. 103 (2008) 07B111.
[32] H.B. Huang, X.Q. Ma, Z.H. Liu, X.M. Shi, T. Yue, Z.H. Xiao, L.Q. Chen, ISRN Condens. Matter. Phys. 2012 (2012) 387380.
[33] D. Houssameddine, U. Ebels, B. Delaët, B. Rodmacq, I. Firastrau, F. Ponthenier, M. Brunet, C. Thirion, J.-P. Michel, L. Prejbeanu-Buda, M.-C. Cyrille, O. Redon, B. Dieny, Nat. Mater. 6 (2007) 441.
[34] Z. Li, S. Zhang, Phys. Rev. B 68 (2003) 024404.